JACS
JOURNAL OF THE AMERICAN CHEMICAL SOCIETY
Article
pubs.acs.org/JACS

Substituent Effects That Control Conjugated Oligomer Conformation through Non-covalent Interactions

Seth A. Sharber,[†] Rom Nath Baral,[†] Fanny Frausto,[†] Terry E. Haas,[†] Peter Müller,[‡] and Samuel W. Thomas III*[,†]

[†]Department of Chemistry, Tufts University, Medford, Massachusetts 02155, United States
[‡]Department of Chemistry, Massachusetts Institute of Technology, Cambridge, Massachusetts 02139, United States

Supporting Information

ABSTRACT: Although understanding the conformations and arrangements of conjugated materials as solids is key to their prospective applications, predictive power over these structural factors remains elusive. In this work, substituent effects tune non-covalent interactions between side-chain fluorinated benzyl esters and main-chain terminal arenes, in turn controlling the conformations and interchromophore aggregation of three-ring phenylene-ethynylenes (PEs). Cofacial fluoroarene−arene (ArF−ArH) interactions cause twisting in the PE backbone, interrupting intramolecular conjugation as well as blocking chromophore aggregation, both of which prevent the typically observed bathochromic shift observed upon transitioning PEs from solution to solid. This work highlights two structural factors that determine whether the ArF−ArH interactions, and the resulting twisted, unaggregated chromophores, occur in these solids: (i) the electron-releasing characteristic of substituents on ArH, with more electron-releasing character favoring ArF−ArH interactions, and (ii) the fluorination pattern of the ArF ring, with 2,3,4,5,6-pentafluorophenyl favoring ArF−ArH interactions over 2,4,6-trifluorophenyl. These trends indicate that considerations of electrostatic complementarity, whether through a polar−π or substituent−substituent mechanism, can serve as an effective design principle in controlling the interaction strengths, and therefore the optoelectronic properties, of these molecules as solids.

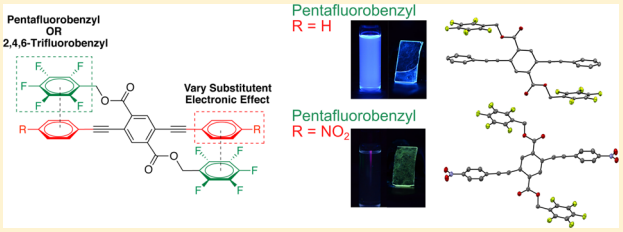

INTRODUCTION

The accurate prediction of the properties of conjugated materials in dilute solution has become relatively straightforward. The rational design of key properties of these materials as solid-state ensembles, however, remains an elusive goal.[1] Control over the optoelectronic behavior of these solids is paramount for efficient function of these materials in their many potential applications. Optical properties of solids depend not only on chemical structures of chromophoric units, but also on conformation and intermolecular coupling, which non-covalent forces can direct. The weak nature of these individual interactions presents a long-standing challenge for understanding the packing of molecules as solids, as well as predicting bulk material properties.

Incorporating directional non-covalent interactions into conjugated molecules offers the potential for dictating conformations and intermolecular packing in crystals and can therefore yield control over optoelectronic properties. For example, hydrogen bonding is a powerful tool in crystal engineering, useful in constructing low-band-gap materials by driving self-assembly across the breadth of the nanoscale: intramolecular hydrogen bonds can restrict conformation and increase conjugation length,[2,3] whereas intermolecular hydrogen bonding can guide formation of molecular assemblies with charge-transfer character and dipolar interactions as well as photoactive nanostructures.[4−6] In addition, halogen bonding offers versatility in interaction directionality and structurally tuned packing motifs,[7] which has proven useful in altering molecular packing for efficient electron transport.[8] Chalcogen interactions have been similarly integrated between chromophoric units to increase backbone coplanarity and intermolecular coupling in conjugated polymers.[9,10]

Fluorine substitution in conjugated systems has been especially useful for controlling molecular assembly through strong interactions between aromatic rings, most notably in the near-sandwich dimer of the perfluoroarene−arene system widely adopted as a supramolecular synthon across materials science and biology.[11−16] Fluoroarene−arene interactions offer reliability[17] and tunability[18,19] in the preferred orientations of conjugated units while making only small steric alterations in fluorine substitution.[15,20] In-depth theoretical studies of the cofacial interactions of substituted arenes and fluorinated arenes have yielded important insights that further our understanding of aromatic interactions.[21,22] Recent efforts have enhanced our understanding of how substituents influence the interactions between aromatic rings beyond the polar−π model by illuminating the importance of dispersion interactions and the local nature of interactions between substituents.[21−33] These considerations are important not only for understanding

Received: January 25, 2017
Published: March 31, 2017

DOI: 10.1021/jacs.7b00878
J. Am. Chem. Soc. 2017, 139, 5164−5174

aromatic interactions but also for manipulating the fluoroarene−arene (ArF−ArH) synthon as a supramolecular control unit.

From the perspective of applications of conjugated materials, oligomers (OPEs) and polymers (PPEs) of phenyleneethynylene (PE)-linked backbones have proven useful in chemical sensors,[34,35] photovoltaics,[36] electronics,[37,38] and solid-state luminescent devices.[39,40] In addition, the low barriers to rotation (~1 kcal/mol) of PE linkages allow for a wide range of accessible conformers both in solution and in the solid state, presenting an opportunity for functional materials as well as a challenge for exerting control over conformation.[41,42] Therefore, the use of chemical structure to bias PE conformation, and the resultant magnitude of electronic coupling, has been important in several breakthroughs in PE chemistry: (i) Rigid, sterically hindered groups such as pentiptycenes prevent interchain aggregation and enable reproducibly bright emission from PPEs for applications in chemoresponsive films and light-emitting devices;[34,43−49] the electronic effects of pentiptycenes can also play key roles in determining conformational preferences of PEs.[50] (ii) Long-lived phosphorescence in tethered, twisted tolanes demonstrates the dramatic dependence of PE photophysics on intramolecular conformation and the utility of biasing geometry.[51−54] (iii) Enforcing coplanarity of the PE backbone through intramolecular hydrogen bonding deepens the potential energy well for PE bond rotation in solution, shifting fluorescence bathochromically.[2,55]

Our group recently reported several examples of three-ring PEs in which discrete interactions between aromatic rings in side chains—the function of which, until recently,[56] has typically been restricted to imparting solubility to otherwise insoluble conjugated materials—and aromatic rings in main chains determined the conformations along the PE backbones in the solid state. Edge−face interactions between nonfluorinated rings reinforced coplanar PE conformations, while cofacial interactions between perfluoroarene pendants[57] and aromatic rings in the conjugated backbones yielded PE chromophores twisted from coplanarity by 55−60° (Figure 1).[58] These changes in PE conformations yielded different optical properties in the solid state, with perfluoroarene pendants yielding hypsochromically shifted optical spectra. Such side-chain-based approaches to control of optical spectra contrast with conventional approaches based on altering the structures of conjugated backbones. Herein we report that substituent effects can tune the strengths of fluoroarene−arene interactions involving the side chains and main chains of this class of PE compounds, strongly influencing PE conformations, interchromophore aggregation, and the resulting properties of solid-state PEs.

RESULTS AND DISCUSSION

PE Design and Synthesis. The core designs of molecules reported herein are symmetrical three-ring PEs comprising a central benzyl terephthalate and identical terminal rings. We targeted two series of molecules in this work, the difference between them being the level of fluorination of the benzyl substituents (the "ArF" ring in ArF−ArH interactions): (i) 2,3,4,5,6-pentafluorobenzyl and (ii) 2,4,6-trifluorobenzyl. In each series, the electronic effect of substituents on the main-chain terminal rings (the "ArH" ring) is varied using different *para* substituents R, ranging from dimethylaniline (σ_p = −0.83), which is reported to participate in a charge-transfer complex with hexafluorobenzene,[21] to nitrobenzene (σ_p = 0.78).[59] The

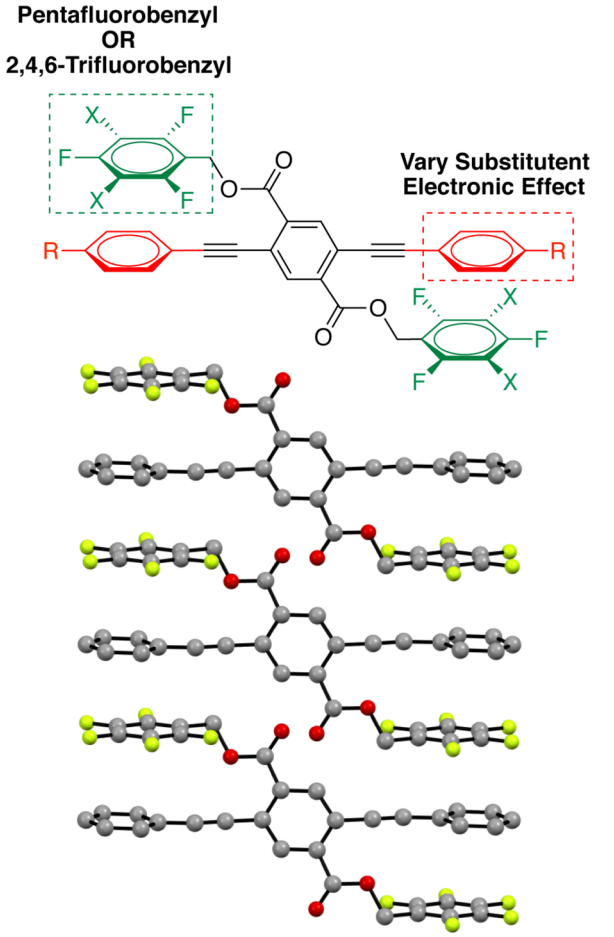

Figure 1. Top: OPE structural perturbations described in this work designed to modify the electrostatic complementarity of cofacially interacting rings. Bottom: X-ray crystal structure of previously reported three-ring OPE **H-F5**, showing how cofacially interacting ArF and ArH rings both yield a twisted (57−58° torsional angles between arenes) conformation and prevent aggregation of PE backbones. Hydrogen atoms have been removed for clarity.

synthesis of these compounds follows a simple sequence of esterification of previously reported[60,61] 2,5-diiodoterephthaloyl chloride with either pentafluorobenzyl alcohol or 2,4,6-trifluorobenzyl alcohol, followed by Sonogashira coupling with the appropriate substituted arylethynylene to yield each target compound (Scheme 1).

Spectroscopy of R-F5 Series. Table 1 summarizes the absorbance and fluorescence spectra of the compounds in the **R-F5** series, with R = NMe_2, OMe, H, CO_2Me, CF_3, CN, and NO_2 as both solutions in chloroform and as drop-cast films. Figure 2 shows spectra for **NMe2-F5**, **CO2Me-F5**, and **NO2-F5** (see the Supporting Information (SI) for spectra of all compounds); Figure 3 shows pictures of the photoluminescence from these solutions and solids. Generally, the trends in spectra of these compounds in dilute organic solution are expected on the basis of simple models of substituent effects. The central terephthalate ring in each of these compounds is a relatively electron-poor unit, enabling donor−acceptor characteristics with relatively electron-rich terminal arenes. Consequently, the absorbance and emission spectra of **NMe2-F5** (436 nm/575 nm) and **OMe-F5** (385 nm/465 nm) were shifted bathochromically relative to the other **R-F5** derivatives (360−373 nm/410−425 nm).

DOI: 10.1021/jacs.7b00878
J. Am. Chem. Soc. 2017, 139, 5164−5174

Scheme 1. Synthesis of Two Series of Three-Ring PEs, R-F5 and R-F3, with R = NMe_2, OMe, H, CO_2Me, CF_3, CN, or NO_2

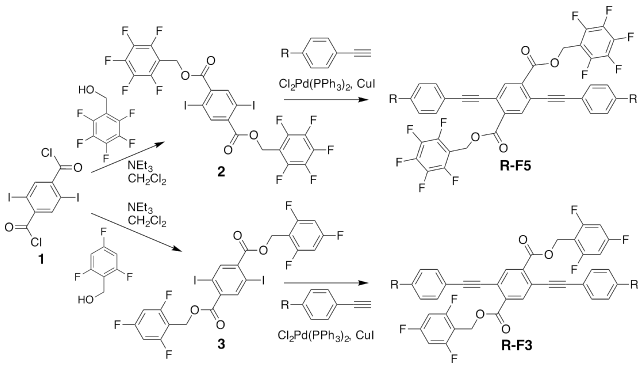

To assess substituent effects on the spectroscopy of these molecules as solids, we prepared thin films by drop casting from chloroform onto planar quartz substrates. As many of these compounds showed polymorphic behavior, we annealed films at 100−115 °C for 15 min, followed by slow cooling to ambient temperature, to ameliorate the issue of preparation-dependent morphologies of the solid samples.[62] Although all data shown here were obtained from drop cast films, thermally annealed spun cast films showed similar behavior. The fluorescence spectra of all **R-F5** compounds were reproducible upon thermal annealing. For example, **CO2Me-F5** forms both violet-emissive and blue-emissive phases in samples of crystals, powders, and films; these samples, however, converge on violet emission after slowly cooling from the melt. In addition, because the crystalline nature of these materials made the acquisition of absorbance spectra difficult due to scattering, we display fluorescence excitation spectra as substitutes. The SI contains absorbance spectra for those samples that yielded reasonably low levels of scattering.

Unlike those of solutions, the absorbance and fluorescence spectra of these molecules as drop-cast thin films did not show a consistent correlation of spectral position with electron-donating ability of the substituents on the terminal rings. Instead, the longest wavelength maxima of absorbance and fluorescence originated from solids with powerful electron donors (R = NMe_2) or powerful electron acceptors (R = CN, NO_2). Especially instructive in this analysis is to correlate the spectral shifts upon transition from solution to solid state, which are shown as individual columns in Table 1. We classify the molecules into two distinct categories on the basis of the spectral shifts observed: (i) a hypsochromic or slight bathochromic shift in absorbance and fluorescence and (ii) a strong bathochromic shift in absorbance and fluorescence.

Molecules in the first category are those in which R is an electron-donating group, hydrogen atom, or a modest electron-withdrawing group (CO_2Me, CF_3). The absence of strong bathochromic shifting upon transitioning to the solid suggests the absence of one or both of the factors that can lead to the well-known bathochromic shifting of PE-based materials—increased coplanarity of conjugated rings or increased interchromophore coupling through aggregation.[63]

Conversely, molecules in the second category showing strong bathochromic shifts in both solid state absorbance (15−40 nm) and fluorescence maxima (>100 nm) are those with either of the two most potent electron-withdrawing groups examined (CN, NO_2). These results suggest that the PE backbones of **CN-F5** and **NO2-F5** are coplanar, aggregated, or both. An interesting effect of this trend is that chromophores with more donor−acceptor character (such as **OMe-F5**) can have larger band gaps than those with less donor−acceptor character (**CN-F5** or **NO2-F5**), contradicting the common paradigm for chromophore design.[64]

Crystallography of R-F5 Series. With the exception of **CN-F5**, we have determined X-ray crystal structures for all compounds in the **F5** series, including for two different polymorphs of **CO2Me-F5**—a violet- and a blue/green-emitting polymorph. Although the structure of **CF3-F5** is a partial structure, it enables us to determine the conformation of the conjugated backbone. As expected on the basis of the spectra described above, all **R-F5** structures except for **NO2-F5** and the blue/green-emitting polymorph of **CO2Me-F5** had packing motifs similar to those described for **OMe-F5** and **H-F5** in our previous report. The most obvious common attribute among these structures is the presence of infinite stacks of arenes comprising intramolecular and intermolecular cofacial ArF−ArH interactions (Figure 4). The three new compounds in the **R-F5** series that show this packing motif—**NMe2-F5**, **CO2Me-F5** (violet), and **CF3-F5**—have geometric parameters consistent with ArF−ArH cofacial interactions, such as closest $C_{ArF}\cdots C_{ArH}$ contacts between 3.4 and 3.5 Å, and centroid-centroid distances of 3.7−3.8 Å. The ArF and ArH rings do not form perfect sandwich dimers, but instead the ArH rings extend out farther from the core terephthalate than the ArF rings by ∼1 Å; such displacements have been calculated to yield larger interaction energies than perfect sandwich dimers due the possibility for closer distances between rings.[21]

Table 1. Absorbance and Emission Parameters for the R-F5 Series of Compounds in $CHCl_3$ and as Thin Films Drop-Cast from $CHCl_3$[a]

	absorbance			emission				
	λ_{max} (nm)			λ_{max} (nm)				
	solution	film	shift (nm)	solution	film	shift (nm)	Φ_F	τ (ns)
NMe2-F5	436	400	−36	575	555	−20	0.26	2.0
OMe-F5	385	375	−10	465	460	−5	0.47	2.5
H-F5	362	342	−20	425	440	15	0.51	1.7
CO2Me-F5	363	338	−25	415	400	−15	0.46	0.7
CF3-F5	360	335	−25	410	390	−20	0.38	0.3
CN-F5	365	380	15	410	520	110	0.48	0.6
NO2-F5	373	415	42	413	525	112	<0.01	–

[a]All thin films were heated to 100 °C for 15 min after solvent evaporated. Reported quantum yields Φ_F and lifetimes τ are for $CHCl_3$ solutions.

DOI: 10.1021/jacs.7b00878
J. Am. Chem. Soc. 2017, 139, 5164−5174

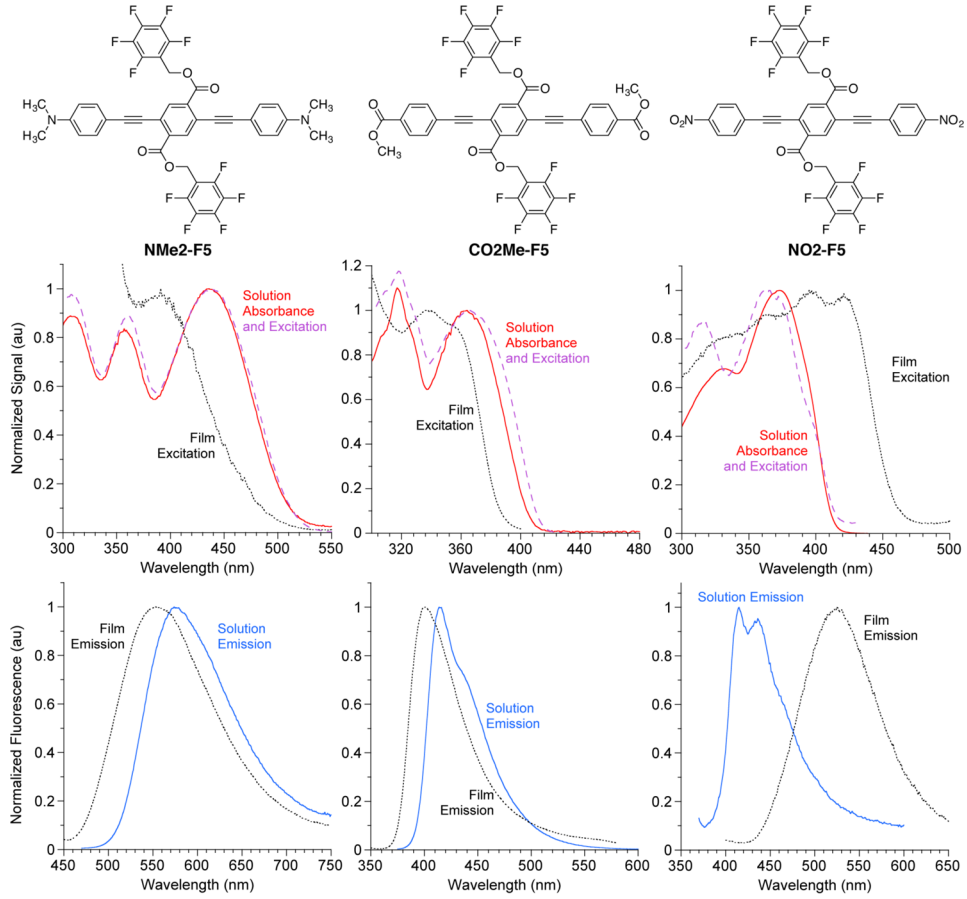

Figure 2. Optical spectra of **NMe2-F5**, **CO2Me-F5**, and **NO2-F5** in chloroform solution and as drop-cast thin films. All thin films were heated to 100 °C for 15 min after solvent evaporated at ambient temperature. Dashed lines are solution excitation spectra.

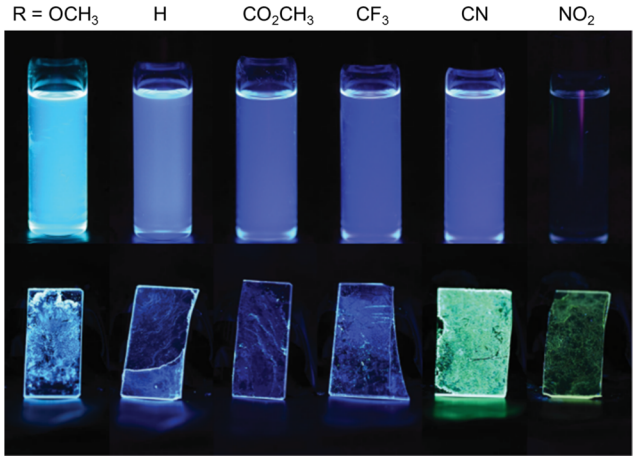

Figure 3. Photographs of fluorescence from solutions ($CHCl_3$) and solids of **R-F5** compounds.

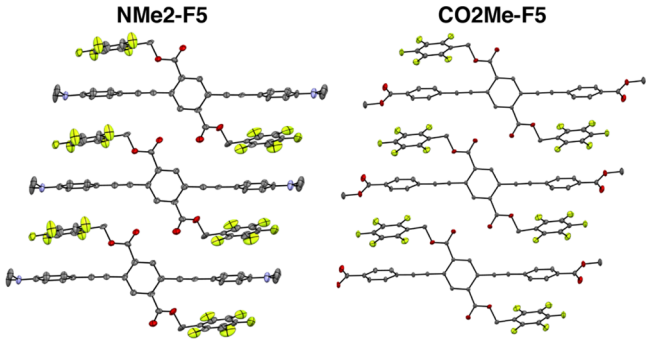

Figure 4. Single-crystal X-ray structures of two compounds in the **R-F5** series that show conserved packing motifs with intramolecular and intermolecular ArF−ArH interactions resulting in twisted PE backbones. Hydrogen atoms have been omitted for clarity. Thermal ellipsoids are shown at 50% probability.

These ArF−ArH interactions play an important role in minimizing intramolecular orbital overlap by enforcing twisted PE backbones, with inter-ring torsional angles of 60−63° (**CF3-F5**), 67−70° (**CO2Me-F5**), and 81−83° (**NMe2-F5**). These favored conformations appear to be due to geometric restrictions imposed by the short benzylic ester tether between the PE backbone and the pentafluorobenzene ring. In all examples of this packing motif, the ester functional groups adopt similar conformations, with the alkoxy groups of the esters oriented *syn* to the alkyne substituents—the opposite rotamers with the alkoxy groups oriented *anti* to the alkyne substituents would not leave sufficient length of the tether for ArF and ArH rings to interact intramolecularly. This geometric restriction is apparent in the crystal structures of two polymorphs of **CO2Me-F5** (*vide infra*), in which the distance between the alkoxy oxygen and the centroid of the nearest terminal PE ring is longer for the coplanar polymorph with *anti* rotamers (7.6 Å) than for the twisted polymorph with *syn* rotamers (5.2 Å). A crystal structure of the coplanar polymorph can be found in the Supporting Information.

DOI: 10.1021/jacs.7b00878
J. Am. Chem. Soc. 2017, 139, 5164−5174

In addition to enforcing highly twisted conformations, cofacial interactions between pendant ArF rings and conjugated ArH rings also preclude interchromophore aggregation. Except for **NO2-F5** and the blue/green-emitting polymorph of **CO2Me-F5**, in no cases did we find any significant intermolecular cofacial interactions of the conjugated PE chains that would be necessary to form J- or H-aggregates.[65] We attribute this to a combination of two factors: (i) the blocking of all faces of the terminal conjugated phenylene rings of these molecules with perfluorinated arenes from non-conjugated pendants, and (ii) shielding of the PE cores by the flanking perfluorinated rings—for example, interactions between fluorine atoms of C–F bonds and the faces of electron poor terephthalates are key short intermolecular contacts between adjacent stacks (Figure 5).

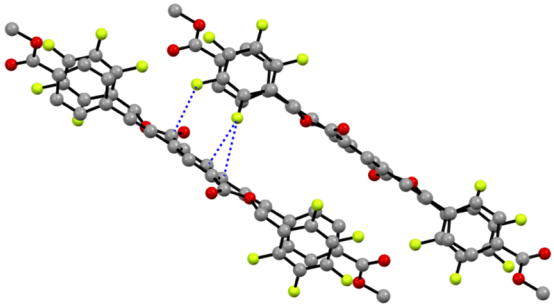

Figure 5. Single-crystal X-ray structure of **CO2Me-F5**, visualized along the crystallographic *b*-axis, highlighting C–F/terephthalate edge-face contacts between stacks of chromophores. Hydrogen atoms have been omitted for clarity.

The crystal structure of **NO2-F5**, however, contrasts strongly with structures in Figures 1 and 4. Although its conjugated PE backbone is twisted, with torsional angles between 62 and 67°, there are no cofacial intramolecular ArF–ArH interactions. The closest intramolecular contact between the two rings is 6.6 Å (Figure 6a). Furthermore, the conformation of the benzoate esters, with the carbonyl groups *syn* to the alkyne substituents on the terephthalate rings, precludes the cofacial interactions observed in the other **R-F5** structures. Because the ArF rings do not effectively enshroud the conjugated backbone, interchain aggregation of PE chromophores take place in **NO2-F5**. Each benzoate ester group interacts cofacially, through complementary dipole–dipole interactions, with both a nitro group on one face and a terephthalate ring on the other face, creating nitro–terephthalate–terephthalate–nitro cofacial stacks throughout the structure (Figure 6b), with C···C, C···O, and N···O intermolecular contacts with distances less than 3.56 Å. Each PE molecule participates in four such stacks, resulting in a network of aggregated chromophores. Lastly, the blue/green-emitting polymorph of **CO2Me-F5** shows both highly coplanar PE chromophores (torsional angles ~2°) and an arrangement of the chromophores in slipped-stacks, enabling electronic coupling between chromophores. A 0.6 eV larger calculated HOMO–LUMO gap from single point energy DFT calculations for the twisted polymorph than for the planar polymorph highlights the importance of conformation of these molecules (SI). Emission from the blue/green-emitting, coplanar polymorph is not observed in annealed thin films, suggesting that the twisted, violet-emitting polymorph is favored.

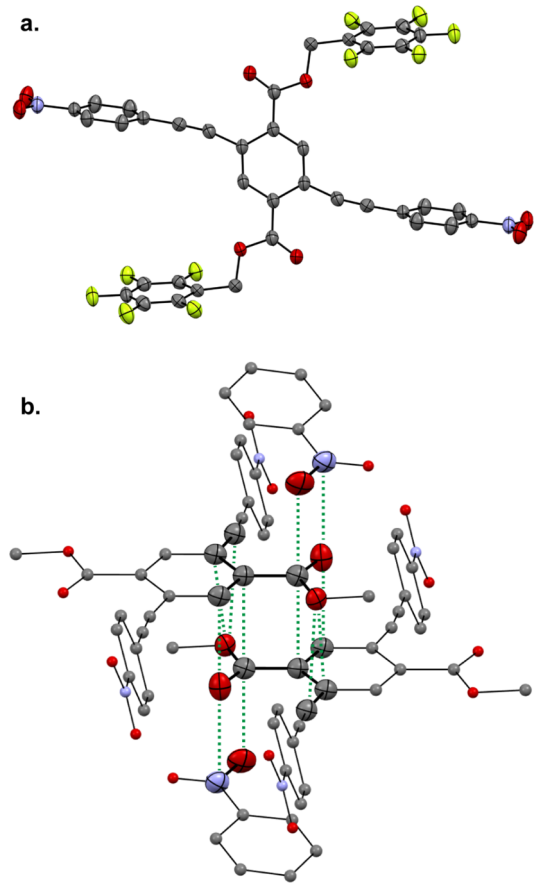

Figure 6. (a) Single-crystal X-ray structure of **NO2-F5**. Hydrogen atoms have been omitted for clarity, and all thermal ellipsoids are displayed at 50% probability. (b) Highlight of nitro–terephthalate–terephthalate–nitro cofacial aggregate motifs; dashed lines indicate interatomic distances <3.56 Å. For clarity, all perfluorobenzene rings have been omitted, as have all atoms except the nitroarene ring from the top and bottom contributors. Atoms that participate in these cofacial stacks are shown as 50% probability thermal ellipsoids; others are shown as small spheres.

We therefore conclude that the behavior of molecules that do not show strong bathochromic shifting is due to inhibition of both (i) interchromophore coupling (aggregation) and (ii) coplanarity of the PE backbones, due to the supramolecular synthon of ArF–ArH interactions between non-conjugated pendants and terminal rings of the PEs. This conclusion is similar to our previous report on a smaller breadth of substituents. In contrast, the strong electron-withdrawing character of the nitro group in **NO2-F5** weakens analogous ArF–ArH cofacial interactions, resulting in other packing arrangements, yielding inter-PE aggregation causing bathochromic shifting of absorbance and emission of films. DFT calculations on an individual molecule of **NO2-F5**, using atomic coordinates identical to those determined from the crystal structure, also support this conclusion. Consistent with the differences of the onset of absorbance spectra in solution, the calculated HOMO–LUMO gap of **NO2-F5** was only ~0.1 eV less than that calculated for individual molecules from the crystal structures of **H-F5** and **CO_2Me-F5** (see SI), suggesting the importance of intermolecular aggregation in the observed solution-to-solid bathochromic shift of **NO2-F5**. We therefore further infer that the cyano group of **CN-F5** also weakens ArF–ArH cofacial interactions sufficiently to disrupt the packing

DOI: 10.1021/jacs.7b00878
J. Am. Chem. Soc. 2017, 139, 5164–5174

Table 2. Absorbance and Emission Parameters for the R-F3 Compounds in $CHCl_3$ and as Drop-Cast Thin Films[a]

	absorbance			emission				
	λ_{max} (nm)			λ_{max} (nm)				
	solution	film	shift (nm)	solution	film	shift (nm)	Φ_F	τ (ns)
NMe2-F3	430	410	−20	565	545	−20	0.39	2.5
OMe-F3	382	350	−32	460	460	0	0.47	2.2
H-F3	363	377	14	420	490	70	0.50	1.0
CO2Me-F3	360	375	15	413	512	99	0.45	1.0
CF3-F3	355	340	−15	405	395/465[b]	−10/60[b]	0.38	0.3
CN-F3	360	375	15	405	505	100	0.52	0.4
NO2-F3	375	400	25	412	540	128	<0.01	–

[a]All thin films were heated to 100 °C for 15 min after solvent evaporated. Reported quantum yields Φ_F and lifetimes τ are for $CHCl_3$ solutions. [b]Two differently emitting polymorphs were observed consistently in thin films.

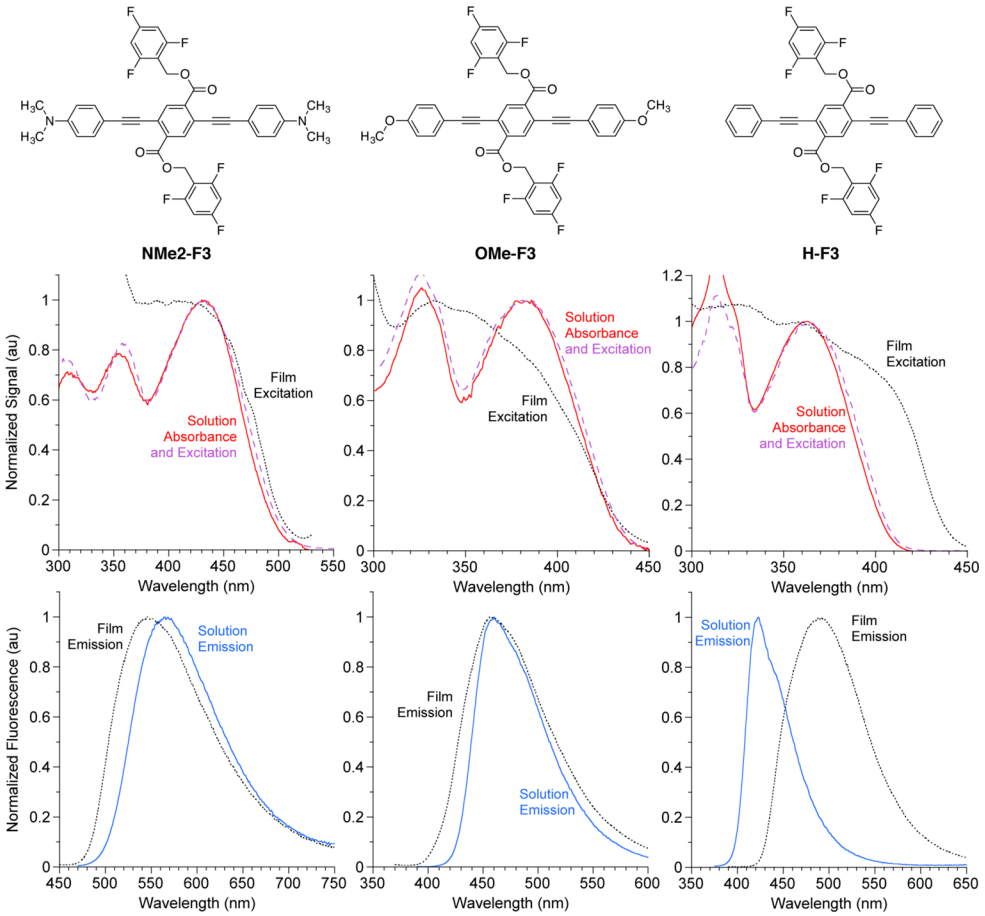

Figure 7. Fluorescence excitation and emission spectra of **NMe2-F3**, **OMe-F3**, and **H-F3** in $CHCl_3$ solution and as thin films drop cast from $CHCl_3$. All thin films were heated to 100 °C for 15 min after solvent evaporated at ambient temperature. Dashed lines are solution excitation spectra.

motif shown in Figures 1 and 3, resulting in PE coplanarity, aggregation, or both.

Spectroscopy of R-F3 Series. Given that substituent effects on ArH rings yield a predictable trend as to whether the ArF−ArH supramolecular synthon dictates the packing of these conjugated molecules, in turn determining their solid-state optical properties, we reasoned that decreasing the level of fluorination of the ArF rings could have a similar effect. We therefore prepared the **R-F3** series of PEs, which substitute 2,4,6-trifluorobenzyl esters for the pentafluorobenzyl esters used in the **R-F5** series. These pendants retain the fluorine in the 4-position, which is usually closest to the *para* substituents on the ArH rings, while potentially changing the strengths of cofacial interactions through replacement of the fluorine atoms in the 3- and 5-positions with hydrogen atoms. We expected this to reduce the ArF−ArH interaction energy for substituted benzenes; in demonstrating the local nature of substituent effects in ArF−ArH interactions, Wheeler and co-workers have shown that the regiochemistry of substituents is key to the strengths of cofacial interactions.[66]

Table 2 and Figure 7 summarize the absorbance and fluorescence spectra of compounds in the **R-F3** series as both dilute chloroform solutions and drop cast thin films (see the SI for the spectra of all molecules); Figure 8 shows photographs of the fluorescence of these samples. Any differences between the solution-phase spectra of these compounds and those of **R-F5**

DOI: 10.1021/jacs.7b00878
J. Am. Chem. Soc. 2017, 139, 5164−5174

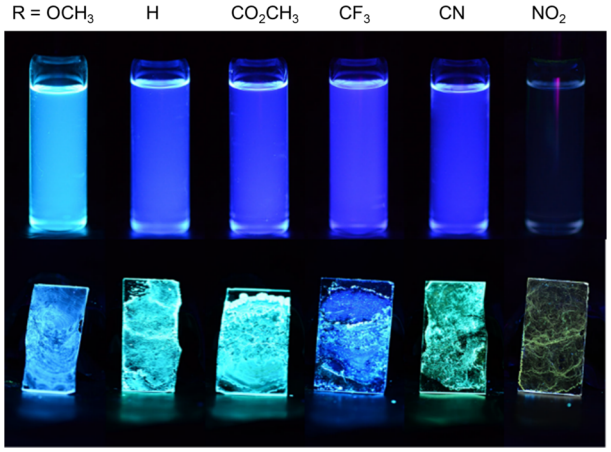

Figure 8. Photographs of the fluorescence of solutions in chloroform and films drop-cast from chloroform demonstrating substituent effect on solid behavior in compounds with 2,4,6-trifluorinated pendants.

compounds with identical conjugated backbones are less than 10 nm. We therefore conclude that effects of the trifluorinated and pentafluorinated arene substituents on the distribution of conformations and the electronic structure of the conjugated chromophore backbones are similar. Although our previous work has demonstrated that inductive effects of analogous non-conjugated pendants on the frontier molecular orbital (FMO) energies of three-ring PEs can occur in solution, such shifts require more significant differences in structures than investigated here.[67]

The absorbance and fluorescence spectra of these compounds as thermally annealed drop-cast thin films show a trend similar to that described above for the **R-F5** series of compounds—substituents that are electron-donating yield hypsochromic shifts in solids relative to spectra in solution, while those that are electron-withdrawing generally yield bathochromic shifts. The key difference between the two series, however, is the point at which this change in behavior occurs. As described above, for the **R-F5** series, it occurs between R = CF_3 (σ_p = 0.54) and R = CN (σ_p = 0.66), with polymorphism that converges on the hypsochromically shifted phase in **CO2Me-F5** and **CF3-F5**. In contrast, for the **R-F3** compounds, this change occurs between R = OCH_3 (σ_p = −0.27) and R = H (σ_p = 0).[59] For example, while **OMe-F3** shows a 30 nm hypsochromic shift of absorbance maxima and no significant shift of emission maxima comparing solid to solution, **H-F3** shows 14 and 70 nm bathochromic shifts, respectively (Figure 7). **R-F3** compounds with $\sigma_p > 0$ show similarly large bathochromic shifts.

An exception to this trend is **CF3-F3**, which has been the only compound investigated in this work that shows persistent polymorphism. Thin films of this compound have emission spectra either bathochromically or hypsochromically shifted from solution, depending on the method of fabrication. For example, slow cooling of **CF3-F3** from the melt results in a solid with violet fluorescence (hypsochromically shifted from solution), blue fluorescence (bathochromically shifted from solution), or both. Films prepared by slow evaporation from dichloromethane emit blue light, while films prepared by slow evaporation from chloroform gave a mixture of both violet- and blue-emitting phases. Complete switching of one phase to the other was not observed upon heating these films to any temperatures below melting (196−198 °C). This behavior contrasts with the analogue **CF3-F5**, which although showing a blue phase bathochromically shifted from solution in freshly prepared films, converges exclusively on the violet-emitting phase upon annealing at 100 °C.

Crystallography of R-F3 Series. Crystallography experiments described below justify extending our model correlating substituent effects, optical spectroscopy, and crystallography to the **R-F3** series. Single-crystal X-ray structures of those compounds that did not show significant bathochromic shifts in optical spectra and had the strongest electron-donating substituents on the ArH rings, in this case **NMe2-F3** and **OMe-F3** have packing motifs similar to those of most of the members of the **R-F5** series, with intramolecular and intermolecular ArF−ArH interactions that extend throughout the structure (Figure 9). In these examples, the ArF rings in each molecule

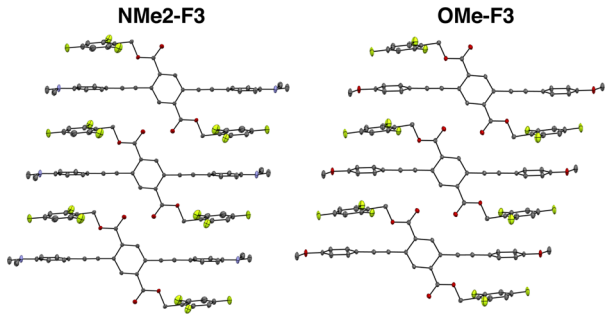

Figure 9. X-ray crystal structures of **NMe2-F3** and **OMe-F3**, with hydrogen atoms omitted. The thermal ellipsoids are shown at 50% probability.

are tilted decidedly toward the ArH rings in the same molecule, resulting in closest C···C distances between the interacting rings of 3.47 Å (**NMe2-F3**) and 3.53 Å (**OMe-F3**), while centroid−centroid distances are 3.91−3.95 Å.

Consistent with our previous observations of this packing motif, the conjugated PE chains of these two molecules are strongly twisted—in these cases they are nearly perpendicular, with torsional angles of 80−82°. Also, hydrogen bonds comprising carbonyl oxygen acceptors and C−H bonds of the 2,4,6-trifluorobenzene rings (C···O distances of 3.25−3.26 Å) exist between adjacent stacks. These interactions appear to be important for preventing aggregation of the PE chromophores. Therefore, the absence of both coplanarity and PE aggregation in these crystal structures is consistent with the lack of strong bathochromic shifts observed in the fluorescence spectra of films.

We have also determined a complete structure for **H-F3** (Figure 10) and a partial structure for **CN-F3**. These crystal structures do not show ArF−ArH cofacial interactions, instead showing PE conformations for **H-F3** (13°−16° torsions) that are generally coplanar. In addition, a partial structure of **CN-F3** suggests torsional angles of 7−8° (see SI). These structures also show substantial overlap between the π-systems of PE backbones in slipped stacks consistent with J-aggregates, with inter-PE C···C distances as short as 3.27 Å and slip angles between stacked PEs of 44−46°. The observations in these crystal structures of geometrical factors commonly implicated in bathochromic shifting of PEs—planarization and aggregation—are therefore consistent with the bathochromic shifting we observe in the **R-F3** compounds for which $\sigma_p \geq 0$.

In addition, we have determined crystal structures for two differentially emissive polymorphs of **CF3-F3**, each of which

DOI: 10.1021/jacs.7b00878
J. Am. Chem. Soc. 2017, 139, 5164−5174

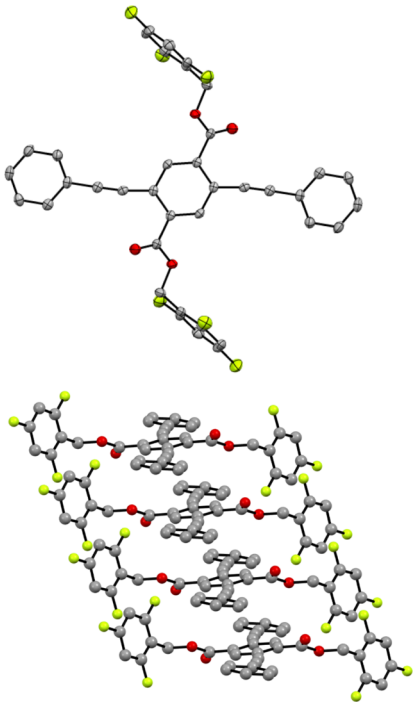

Figure 10. Two views of the X-ray crystal structure of **H-F3**, with hydrogen atoms omitted for clarity. Thermal ellipsoids in top image are shown at 50% probability.

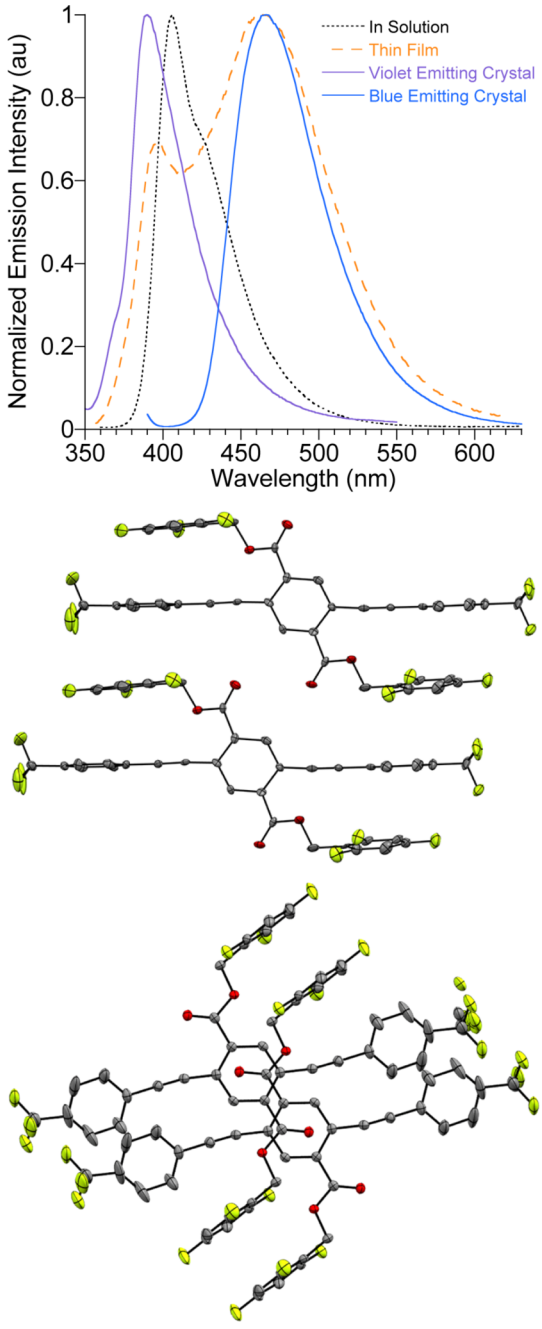

Figure 11. Top: Fluorescence emission spectra of **CF3-F3** in dilute chloroform solution, as a thermally annealed drop-cast thin film, and of two polymorphic single crystals. Middle and bottom: X-ray crystal structures of the violet- (middle) and blue-emitting single-crystal polymorphs of **CF3-F3**. Hydrogen atoms have been omitted for clarity. Thermal ellipsoids are shown at 50% probability.

shows packing motifs consistent with those described above. The emission spectra of each of the two crystals show excellent spectral match with one of the two emission bands observed from thin films (Figure 11). Diffusion of cyclohexane into a concentrated solution of **CF3-F3** in chloroform yielded a violet-emitting prism, the crystal structure of which shows the twisted PE motif enforced by ArF−ArH interactions, together with C−H/π and hydrogen-bonding interactions, similar to **NMe2-F3** and **OMe-F3**. Conversely, slow evaporation of dichloromethane with layered hexanes yielded a blue-emitting crystal, the crystal structure of which has highly planarized PE backbones and intermolecular stacking contacts consistent with J-aggregation, similar to **H-F3** and **CN-F3**. Consistent in both crystal structures are apparent F···F interactions between terminal trifluoromethyl groups (F···F distances as close as 2.84 Å), suggesting that the inclusion of other competitive non-covalent interactions influences crystal packing of these molecules, especially with reduced interaction energy for the ArF−ArH cofacial interactions relative to more electron-donating substituents.

Summary of Structure−Property Relationships in R-F5 and R-F3 Compounds. The similarities of these two series of molecules are extensive, as they differ only in the degree of fluorination of the benzylic ester groups, which are not π-conjugated to the PE backbone. The lack of significant change in solution-phase spectra between **R-F5** and analogous **R-F3** derivatives highlights the subtle nature of this chemical change, relative to the manner by which the electronic structures of conjugated materials are typically tuned. In contrast, the behavior of these materials as solids, the required state for most applications of conjugated materials, depends strongly on specific non-covalent interactions of the side chains and main chains. We note several trends connecting chemical structure, crystal structure, and spectroscopy of these two series of compounds:

1. Optical spectra depend critically on whether cofacial ArF−ArH interactions occur between the fluorinated aromatic pendants and terminal rings of the PE backbones. In all cases described above for which these discrete non-covalent interactions occur, the optical spectra of the solids are not significantly batho-chromically shifted from solution. The crystallographic evidence suggests that this feature is due to a

DOI: 10.1021/jacs.7b00878
J. Am. Chem. Soc. 2017, 139, 5164−5174

combination of two factors: (i) twisting of the PE backbones induced by the ArF−ArH interactions, with torsional angles between 55 and 83°, and (ii) insulation of the PE backbones from interchromophore aggregation. Conversely, in all cases in which the ArF−ArH side-chain/main-chain interactions do not take place, significant bathochromic shifting of the PE optical spectra occurs in the solid state. On the basis of the crystal structures of such compounds, we attribute these observations to interchromophore aggregation, PE planarization, or both.

2. The presence or absence of side-chain/main-chain ArF−ArH interactions correlates with the electronic effect of the substituent in monosubstituted ArH rings. In the **R-F5** series of compounds, the *para* substituent of the ArH rings is key in the relative strengths of the ArF−ArH interaction, with the traditional Hammett coefficient serving as an empirically suitable parameter to correlate with our observations. For each series, substituents with smaller σ_p values (larger interaction energies) showed ArF−ArH interactions, while those with larger σ_p values (smaller interaction energies) lacked ArF−ArH interactions; shifts in optical spectra followed these trends, as described in point 1 above (Figure 12). Although dispersion interactions also play a key role in ArF−ArH interactions generally, including in observed substituent effects, our observed trend concerning traditional Hammett-style substituent effects is in line with previous experimental and theoretical studies of ArF−ArH interactions of monosubstituted ArH rings. We have used the σ_p parameter throughout this paper, as it captures more accurately the order of substituent effects in the **R-F3** series (particularly for R = OCH_3), and predicts more closely the trend of calculated ArF−ArH interaction energies, as reported by Wheeler and Houk,[68] for the particular group of substituents chosen for this study. Although the interacting rings in this paper are displaced in at least one dimension, instead of a perfect sandwich dimer as modeled by Wheeler and Houk,[68] Gung and Amicangelo have shown that such correlations persist in parallel displaced interaction geometries using singly substituted ArH rings.[21]
3. The threshold of electronic substituent effect of ArH rings necessary to induce ArF−ArH interactions depends on the fluorination pattern of the ArF rings. Consistent with the idea that there is a significant electrostatic component to the substituent effects observed here, reducing the degree of fluorination of the ArF rings of the pendants generally requires increased electron-donating character of the ArH substituent to observe ArF−ArH interactions and prevent chromophore aggregation. The complex environment of the crystal lattice makes it difficult to ascribe this observation to one particular cause, as numerous factors are changing with this simple chemical modification, including: (i) reduced complementarity of local substituent−substituent and substituent−ring interactions of the ArF−ArH rings, (ii) reduced complementarity of potential polar−π interactions in the cofacial geometry, (iii) the potential for additional non-covalent interactions, such as C−H hydrogen bond donation from the ArF rings, and (iv) changes in the magnitude of dispersion interactions due to the C−H for C−F substitutions.

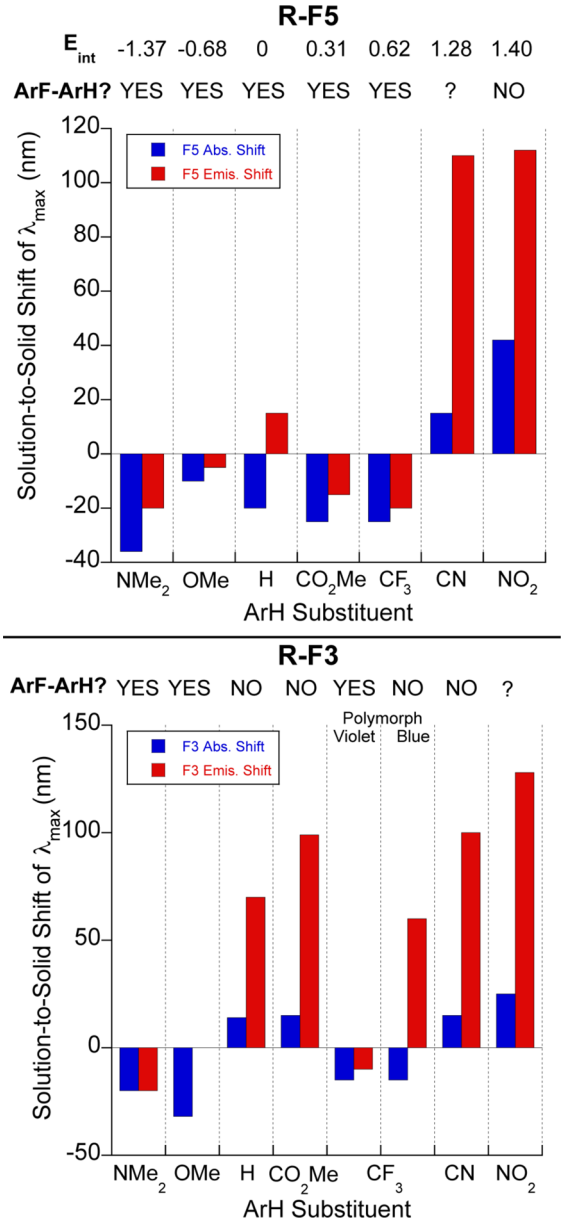

Figure 12. Correlation of (i) observed solution-to-solid shift of absorbance and fluorescence emission spectra, (ii) appearance of side-chain/main-chain ArF−ArH interactions in single-crystal X-ray structures, and (iii) calculated interaction energy, relative to R = H, for the ArF−ArH sandwich dimer, as published by Wheeler and Houk.[68] These data are summarized for both the **R-F5** series (top) and **R-F3** series (bottom) of compounds.

CONCLUSION

This work presents practical outcomes in solid-state functional materials from the extensive theoretical and experimental work regarding substituent effects in the non-covalent interactions of aromatic rings. The low barriers to rotation and known sensitivity to both conformational changes and intermolecular aggregation make phenylene-ethynylenes an ideal class of materials for exploring these concepts. In these examples, substituent effects play a key role in determining whether ArF−ArH interactions are present, which has important consequences for the conformations and electronic structures of these solids. Although the factors governing the strengths of these cofacial interactions are complex, we find here that substituent

DOI: 10.1021/jacs.7b00878
J. Am. Chem. Soc. 2017, 139, 5164−5174

electronic effects of the ArH ring provide a useful structure−property trend regarding whether ArF−ArH interactions occur in structurally analogous PEs. In addition, this concept of complementarity of the ArF and ArH rings can extend to ArF rings with a smaller extent of fluorination, with larger apparent electrostatic substituent effects from the ArH ring required to observe ArF−ArH interactions consistently.

Many of the efforts and successes in the field of conjugated materials have originated from designing, tuning, and optimizing the connectivity of only those atoms and groups that are part of the π-conjugated portions of small molecules and polymers, while side chains are often included only as a necessity to enable solubility. This work highlights that discrete, rationally designed non-covalent interactions of non-conjugated substituents can have dramatic effects on solid-state properties by dictating conformations and interchain packing of conjugated materials. It is currently not clear, however, to what extent these design principles will extend to other classes of conjugated systems. Ongoing topics of research under consideration in our laboratory involve the potential to harness the local nature of substituent effects through regiochemistry of substitution, the extent to which such interactions between side chains and main chains persist as the number of repeating units along the conjugated backbone increases, and the role, if any, that the strength of these interactions has in the sensitivity of optical properties to applied mechanical force.

■ ASSOCIATED CONTENT

Supporting Information

The Supporting Information is available free of charge on the ACS Publications website at DOI: 10.1021/jacs.7b00878.

Full experimental section including detailed descriptions of synthesis, NMR spectra, optical spectra, and descriptions of crystallography (PDF)

X-ray crystallographic data for **NMe2-F5** (CIF)

X-ray crystallographic data for **CO2Me-F5** (violet fluorescence) (CIF)

X-ray crystallographic data for **CO2Me-F5** (blue fluorescence) (CIF)

X-ray crystallographic data for **CF3-F5** (CIF)

X-ray crystallographic data for **NO2-F5** (CIF)

X-ray crystallographic data for **NMe2-F3** (CIF)

X-ray crystallographic data for **OMe-F3** (CIF)

X-ray crystallographic data for **H-F3** (CIF)

X-ray crystallographic data for **CO2Me-F3** (CIF)

X-ray crystallographic data for **CF3-F3** (violet fluorescence) (CIF)

X-ray crystallographic data for **CF3-F3** (blue fluorescence) (CIF)

X-ray crystallographic data for **CN-F3** (CIF)

■ AUTHOR INFORMATION

Corresponding Author

*sam.thomas@tufts.edu

ORCID

Samuel W. Thomas III: 0000-0002-0811-9781

Notes

The authors declare no competing financial interest.

■ ACKNOWLEDGMENTS

The authors thank the U.S. Department of Energy, Basic Energy Sciences (DE-SC0016423), for generous support of this research. Data for X-ray crystal structures were obtained on instrumentation supported by the National Science Foundation (CHE-1229426).

■ REFERENCES

(1) Sutton, C.; Risko, C.; Bredas, J. L. *Chem. Mater.* **2016**, *28*, 3−16.

(2) Hu, W.; Yan, Q. F.; Zhao, D. H. *Chem. - Eur. J.* **2011**, *17*, 7087−7094.

(3) Hoogboom, J.; Swager, T. M. *J. Am. Chem. Soc.* **2006**, *128*, 15058−15059.

(4) Kapadia, P. P.; Ditzler, L. R.; Baltrusaitis, J.; Swenson, D. C.; Tivanski, A. V.; Pigge, F. C. *J. Am. Chem. Soc.* **2011**, *133*, 8490−8493.

(5) Koren, A. B.; Curtis, M. D.; Francis, A. H.; Kampf, J. W. *J. Am. Chem. Soc.* **2003**, *125*, 5040−5050.

(6) Yoosaf, K.; Belbakra, A.; Llanes-Pallas, A.; Bonifazi, D.; Armaroli, N. *Pure Appl. Chem.* **2011**, *83*, 899−912.

(7) Mukherjee, A. *Cryst. Growth Des.* **2015**, *15*, 3076−3085.

(8) Kumar, Y.; Kumar, S.; Keshri, S. K.; Shukla, J.; Singh, S. S.; Thakur, T. S.; Denti, M.; Facchetti, A.; Mukhopadhyay, P. *Org. Lett.* **2016**, *18*, 472−475.

(9) Li, Y. X.; Lee, T. H.; Park, S. Y.; Uddin, M. A.; Kim, T.; Hwang, S.; Kim, J. Y.; Woo, H. Y. *Polym. Chem.* **2016**, *7*, 4638−4646.

(10) Uddin, M. A.; Lee, T. H.; Xu, S.; Park, S. Y.; Kim, T.; Song, S.; Nguyen, T. L.; Ko, S. J.; Hwang, S.; Kim, J. Y.; Woo, H. Y. *Chem. Mater.* **2015**, *27*, 5997−6007.

(11) Coates, G. W.; Dunn, A. R.; Henling, L. M.; Dougherty, D. A.; Grubbs, R. H. *Angew. Chem., Int. Ed. Engl.* **1997**, *36*, 248−251.

(12) Dai, C. Y.; Nguyen, P.; Marder, T. B.; Scott, A. J.; Clegg, W.; Viney, C. *Chem. Commun.* **1999**, 2493−2494.

(13) Kilbinger, A. F. M.; Grubbs, R. H. *Angew. Chem., Int. Ed.* **2002**, *41*, 1563−1566.

(14) Salonen, L. M.; Ellermann, M.; Diederich, F. *Angew. Chem., Int. Ed.* **2011**, *50*, 4808−4842.

(15) Pace, C. J.; Gao, J. M. *Acc. Chem. Res.* **2013**, *46*, 907−915.

(16) Berger, R.; Resnati, G.; Metrangolo, P.; Weber, E.; Hulliger, J. *Chem. Soc. Rev.* **2011**, *40*, 3496−3508.

(17) Ponzini, F.; Zagha, R.; Hardcastle, K.; Siegel, J. S. *Angew. Chem., Int. Ed.* **2000**, *39*, 2323−2325.

(18) Dou, J. H.; Zheng, Y. Q.; Yao, Z. F.; Yu, Z. A.; Lei, T.; Shen, X. X.; Luo, X. Y.; Sun, J. L.; Zhang, S. D.; Ding, Y. F.; Han, G. C.; Yi, Y. P.; Wang, J. Y.; Pei, J. *J. Am. Chem. Soc.* **2015**, *137*, 15947−15956.

(19) Zhu, L. Y.; Tong, F.; Salinas, C.; Al-Muhanna, M. K.; Tham, F. S.; Kisailus, D.; Al-Kaysi, R. O.; Bardeen, C. J. *Chem. Mater.* **2014**, *26*, 6007−6015.

(20) Reichenbacher, K.; Suss, H. I.; Hulliger, J. *Chem. Soc. Rev.* **2005**, *34*, 22−30.

(21) Gung, B. W.; Amicangelo, J. C. *J. Org. Chem.* **2006**, *71*, 9261−9270.

(22) Wheeler, S. E. *J. Am. Chem. Soc.* **2011**, *133*, 10262−10274.

(23) Hwang, J. W.; Dial, B. E.; Li, P.; Kozik, M. E.; Smith, M. D.; Shimizu, K. D. *Chem. Sci.* **2015**, *6*, 4358−4364.

(24) Parrish, R. M.; Sherrill, C. D. *J. Am. Chem. Soc.* **2014**, *136*, 17386−17389.

(25) Hwang, J.; Li, P.; Carroll, W. R.; Smith, M. D.; Pellechia, P. J.; Shimizu, K. D. *J. Am. Chem. Soc.* **2014**, *136*, 14060−14067.

(26) Garcia, A. M.; Determan, J. J.; Janesko, B. G. *J. Phys. Chem. A* **2014**, *118*, 3344−3350.

(27) Ehrlich, S.; Moellmann, J.; Grimme, S. *Acc. Chem. Res.* **2013**, *46*, 916−926.

(28) Sherrill, C. D. *Acc. Chem. Res.* **2013**, *46*, 1020−1028.

(29) Watt, M.; Hardebeck, L. K. E.; Kirkpatrick, C. C.; Lewis, M. *J. Am. Chem. Soc.* **2011**, *133*, 3854−3862.

(30) Ringer, A. L.; Sherrill, C. D. *J. Am. Chem. Soc.* **2009**, *131*, 4574−4575.

DOI: 10.1021/jacs.7b00878
J. Am. Chem. Soc. 2017, 139, 5164−5174

(31) Arnstein, S. A.; Sherrill, C. D. *Phys. Chem. Chem. Phys.* **2008**, *10*, 2646−2655.
(32) Cockroft, S. L.; Perkins, J.; Zonta, C.; Adams, H.; Spey, S. E.; Low, C. M. R.; Vinter, J. G.; Lawson, K. R.; Urch, C. J.; Hunter, C. A. *Org. Biomol. Chem.* **2007**, *5*, 1062−1080.
(33) Sinnokrot, M. O.; Sherrill, C. D. *J. Am. Chem. Soc.* **2004**, *126*, 7690−7697.
(34) Yang, J. S.; Swager, T. M. *J. Am. Chem. Soc.* **1998**, *120*, 11864−11873.
(35) Bunz, U. H. F.; Seehafer, K.; Bender, M.; Porz, M. *Chem. Soc. Rev.* **2015**, *44*, 4322−4336.
(36) Wang, H. Y.; Ding, Y. M.; Lai, Y. B.; Sun, Z. W.; Liu, Y.; Jiang, B.; Chen, M.; Yao, J.; Liu, F.; Russell, T. P. *J. Mater. Chem. A* **2015**, *3*, 12972−12981.
(37) Li, Y. W.; Zhao, J. W.; Yin, G. P. *Comput. Mater. Sci.* **2007**, *39*, 775−781.
(38) Schmid, S.; Kast, A. K.; Schroder, R. R.; Bunz, U. H. F.; Melzer, C. *Macromol. Rapid Commun.* **2014**, *35*, 1770−1775.
(39) Wang, Y. Q.; Park, J. S.; Leech, J. P.; Miao, S.; Bunz, U. H. F. *Macromolecules* **2007**, *40*, 1843−1850.
(40) Breen, C. A.; Tischler, J. R.; Bulovic, V.; Swager, T. M. *Adv. Mater.* **2005**, *17*, 1981−1985.
(41) Levitus, M.; Schmieder, K.; Ricks, H.; Shimizu, K. D.; Bunz, U. H. F.; Garcia-Garibay, M. A. *J. Am. Chem. Soc.* **2001**, *123*, 4259−4265.
(42) Levitus, M.; Zepeda, G.; Dang, H.; Godinez, C.; Khuong, T. A. V.; Schmieder, K.; Garcia-Garibay, M. A. *J. Org. Chem.* **2001**, *66*, 3188−3195.
(43) Swager, T. M. *Acc. Chem. Res.* **2008**, *41*, 1181−1189.
(44) Hughs, M.; Jimenez, M.; Khan, S.; Garcia-Garibay, M. A. *J. Org. Chem.* **2013**, *78*, 5293−5302.
(45) Rose, A.; Zhu, Z. G.; Madigan, C. F.; Swager, T. M.; Bulovic, V. *Nature* **2005**, *434*, 876−879.
(46) Breen, C. A.; Rifai, S.; Bulovic, V.; Swager, T. M. *Nano Lett.* **2005**, *5*, 1597−1601.
(47) Lin, C. J.; Chen, C. Y.; Kundu, S. K.; Yang, J. S. *Inorg. Chem.* **2014**, *53*, 737−745.
(48) Matsunaga, Y.; Yang, J. S. *Angew. Chem., Int. Ed.* **2015**, *54*, 7985−7989.
(49) Englert, B. C.; Smith, M. D.; Hardcastle, K. I.; Bunz, U. H. F. *Macromolecules* **2004**, *37*, 8212−8221.
(50) Lin, C. J.; Kundu, S. K.; Lin, C. K.; Yang, J. S. *Chem. - Eur. J.* **2014**, *20*, 14826−14833.
(51) Brizius, G.; Billingsley, K.; Smith, M. D.; Bunz, U. H. F. *Org. Lett.* **2003**, *5*, 3951−3954.
(52) Menning, S.; Kramer, M.; Duckworth, A.; Rominger, F.; Beeby, A.; Dreuw, A.; Bunz, U. H. F. *J. Org. Chem.* **2014**, *79*, 6571−6578.
(53) Menning, S.; Kramer, M.; Coombs, B. A.; Rominger, F.; Beeby, A.; Dreuw, A.; Bunz, U. H. F. *J. Am. Chem. Soc.* **2013**, *135*, 2160−2163.
(54) Hong, J. H.; Atta, A. K.; Jung, K. B.; Kim, S. B.; Heo, J.; Cho, D. G. *Org. Lett.* **2015**, *17*, 6222−6225.
(55) Hu, W.; Zhu, N. B.; Tang, W.; Zhao, D. H. *Org. Lett.* **2008**, *10*, 2669−2672.
(56) Mei, J. G.; Bao, Z. N. *Chem. Mater.* **2014**, *26*, 604−615.
(57) Patrick, C. R.; Prosser, G. S. *Nature* **1960**, *187*, 1021.
(58) Pawle, R. H.; Haas, T. E.; Muller, P.; Thomas, S. W., III *Chem. Sci.* **2014**, *5*, 4184−4188.
(59) Hansch, C.; Leo, A.; Taft, R. W. *Chem. Rev.* **1991**, *91*, 165−195.
(60) Zhou, Q.; Swager, T. M. *J. Am. Chem. Soc.* **1995**, *117*, 12593−12602.
(61) Huang, W. Y.; Chen, H. Y. *Macromolecules* **2013**, *46*, 2032−2037.
(62) Butler, T.; Morris, W. A.; Samonina-Kosicka, J.; Fraser, C. L. *ACS Appl. Mater. Interfaces* **2016**, *8*, 1242−1251.
(63) Bunz, U. H. F. *Macromol. Rapid Commun.* **2009**, *30*, 772−805.
(64) Pandey, L.; Risko, C.; Norton, J. E.; Brédas, J.-L. *Macromolecules* **2012**, *45*, 6405−6414.
(65) Würthner, F.; Kaiser, T. E.; Saha-Möller, C. R. *Angew. Chem., Int. Ed.* **2011**, *50*, 3376−3410.
(66) Wheeler, S. E.; Bloom, J. W. G. *J. Phys. Chem. A* **2014**, *118*, 6133−6147.
(67) Pawle, R. H.; Agarwal, A.; Malveira, S.; Smith, Z. C.; Thomas, S. W. *Macromolecules* **2014**, *47*, 2250−2256.
(68) Wheeler, S. E.; Houk, K. N. *J. Am. Chem. Soc.* **2008**, *130*, 10854−10855.

DOI: 10.1021/jacs.7b00878
J. Am. Chem. Soc. 2017, 139, 5164−5174